An Adaptive Skin Detection Approach of Face Images with Unequal Luminance, Color Excursion, and Background Interference

Wei Li*, Jian Luo & YanMei Li

Computer School, China West Normal University, Nanchong 637000, China
*E-mail: nos036@163.com

Abstract. Face detection and recognition are affected greatly by unequal luminance, color excursion and background interference. For improving skin detection rates of color face images in the presence of unequal luminance, color excursion and background interference, this paper proposes an approach for automatic skin detection. This approach globally corrects the color excursion using the X, Y, Z color components. Then it establishes a self-adaptive nonlinear amendment function using the a', b' and L' components, and locally corrects the R, G, B color components of row-column transformed sub-block images to balance the global luminance and color. Finally, it constructs an L'a'b' three-dimensional semi-supervised dual-probability skin model, based on which automatic skin detection can be realized. The experimental results demonstrated that this approach has great adaptability, a high detection rate and speed.

Keywords: *color excursion; Lab; skin detection; skin model; unequal luminance.*

1 Introduction

In the fields of pattern recognition and machine vision there are many approaches of face detection and recognition based on appearance, such as methods based on skin model, deep learning, neural network, SVM, Adaboost, feature space, non-negative matrix, etc. [1-22]. Using deep learning and neural network to help realizing face detection or recognition are popular methods [1-3]. But in these types of methods, training of intelligent behavior can only be done offline. The learning/training takes time and relies on hardware. Its performance depends too much on the technique of adjusting the parameters and it is not good at solving certain specific problems. Besides, the training of complex models is very unstable.

Face detection approaches based on skin models are typically approaches based on a number of key features. They generally construct a skin model [4-15] using the clustering distribution of skin tones in the color space in order to detect skin. These approaches calculate quickly and are not easily affected by factors such as expression, posture and rotation but are easily affected by unequal luminance, different color excursions, and background interference [16-18]. Some studies

Received March 11th, 2018, Revised May 25th, 2018, Accepted for publication September 12th, 2018..
 ISSN: 2337-5779, DOI: 10.5614/j.eng.technol.sci.2018.50.4.4

have provided methods based on multiple features, such as illumination-insensitive features, multi-stage kernel probability mapping, multiple feature subspace analysis, hybrid color space strategy [19-22]. Because of their complexity, these methods are limited by the speed at the software level and need better hardware support. So their performance is affected easily by the degree of fusion and complexity.

Among classical approaches based on skin models, Ref. [4] presents an approach of weakening the influence of highlights in the TSL color space that does not weaken the influence of shadows. Ref. [5] provides an approach of nonlinear transformation based on a logarithm in order to adjust brightness and weaken highlights and shadows. However, this process is only aimed at grayscale images that do not contain color information and moreover it adopted a fixed threshold division. Ref. [6] removed color excursion with reference white and also adjusted color and luminance with nonlinear transformation. However, because of using a fixed threshold value, its self-adaptation needs to be improved and the balance ability of color or luminance is limited. Owing to the influence of unequal luminance and color excursion, the detected skin based on a CbCr ellipse skin model may still contain skin-similar regions. There are some situations of over-segmentation and under-segmentation in the approach of skin detection based on an ellipse skin model.

An additional technique is needed, such as grouped regions, to further obtain the face targets. In order to improve the color image skin detection rate, self-adaptation and capacity to resist disturbance, while also reducing the negative influence of color excursion, unequal luminance, and background interference, this paper provides a self-adaptive approach of automatic skin detection that is beneficial for detection of face and facial feature targets. In this study, firstly a self-adaptive global color correction pretreatment is realized using X, Y, Z color components. Secondly, a self-adaptive nonlinear amendment function based on L', a', b' color components is constructed and used to finish the adaptive local illumination-color balance pretreatment for row-column transformed sub-block images. Then, the global image is recovered. Finally, an L'a'b' 3D semi-supervised dual-probability skin model is constructed to realize skin detection.

2 Methodology of Facial Skin Detection

In normal cases, a face recognition approach based on skin detection includes the following elements: image input, image pretreatment, skin modeling and detection, face detection and identification, as shown in Figure 1. The proposed improved approach of skin detection complements the functions of input image pretreatment, skin modeling and detection. The pretreatment involves color excursion correction in two parts as well as luminance-color balancing. Color

excursion correction is done to correct color shifting caused by colored luminance. Luminance-color balancing is done to balance uneven illumination and color, as well as to normalize or stretch luminance. The purpose of luminance-color balancing is to reduce the influence of highlights and shadows as well as to adjust color variation caused by the illumination or the device, in order to restore the actual color in highlight and shadow regions. The skin modeling and detection is mainly done to construct a well-adapted and anti-interference skin model based on the statistical parameters of the skin tone distribution of the training sample and then to use this skin model for calculating skin similarity and segmenting skin regions.

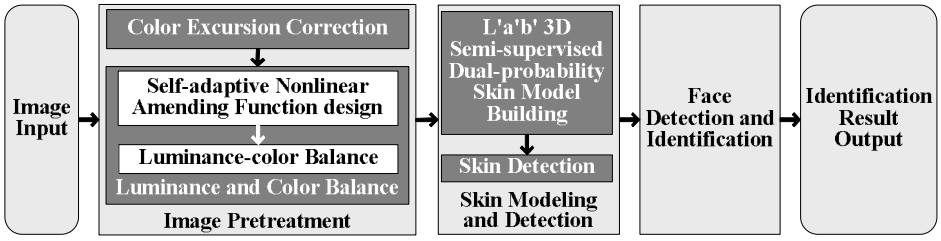

Figure 1 Overall flow of face recognition.

3 Pretreatment of Color Excursion Correction

3.1 Principle and Process of Color Correction Method

Widely used color models include computational color models (also called chroma color models, e.g. RGB, XYZ, Luv, LCH, LAB, UCS, UVW of CIE), industrial color models (e.g. RGB, YUV, YIQ, CMYK, YCbCr of NTSC), visual color models (e.g. HSL, HSV(B)). After a large number of normal human visual and statistical measurements, the CIE (International Lighting Committee) introduced the XYZ color model, a new chroma system using three ideal primary colors (X, Y, and Z) based on the RGB system. Matching the three stimulus values of an equal energy spectrum, they are called the three stimulus values of the CIE1931 standard colorimetric observer spectrum, abbreviated as CIE1931 standard colorimetric observer. CIEXYZ color space is device-independent, containing all the colors that the human eye can perceive. This study adopted the XYZ color model, which is distributed strictly according to the sensitivity of the human eye to the light signal.

This article proposes a new self-adaptive pretreatment of color-excursion correction based on the XYZ color model. In the pretreatment, by using the X, Y, Z color components in the XYZ color space and the accumulated values of each component as well as the average value of the accumulations, the global

color correction coefficients are acquired. Using these color correction coefficients, the X, Y, Z components are adjusted. Next, the XYZ space is transformed into RGB space in order to acquire the color-corrected image. The steps of global color excursion correction are as follows:

1. After bilateral filtering, convert the RGB color format of the input image to the X'Y'Z' color format with Eqs. (1) and (2).

$$\begin{bmatrix} X \\ Y \\ Z \end{bmatrix} = \begin{bmatrix} 0.412453 & 0.357580 & 0.180423 \\ 0.212671 & 0.715160 & 0.072169 \\ 0.019334 & 0.119193 & 0.950227 \end{bmatrix} \begin{bmatrix} R \\ G \\ B \end{bmatrix} \tag{1}$$

$$\begin{bmatrix} X' \\ Y' \\ Z' \end{bmatrix} = \begin{bmatrix} (X/(255 \times 0.950456) \\ Y/(255) \\ Z/(255 \times 1.088754) \end{bmatrix} \tag{2}$$

2. Accumulate the X', Y', Z' components respectively and acquire three average values $\bar{X}, \bar{Y}, \bar{Z}$. Then calculate the average value (cXYZ) of $\bar{X}, \bar{Y}$, $\bar{Z}$ and adjustment the coefficients (cX, cY, cZ) of each component (X', Y', Z').

$$cXYZ = \frac{\left(\bar{X} + \bar{Y} + \bar{Z}\right)}{3}, cX = \frac{cXYZ}{\bar{X}}, cY = \frac{cXYZ}{\bar{Y}}, cZ = \frac{cXYZ}{\bar{Z}} \tag{3}$$

3. Adjust the X', Y', Z' components (converted by Eqs. (1) and (2)) using three adjustment coefficients cX, cY, cZ according to Eq. (4):

$$X'' = X' \times cX, \quad Y'' = Y' \times cY, \quad Z'' = Z' \times cZ \tag{4}$$

4. Convert the adjusted X", Y", Z" components to R', G', B' according to Formula (5).

$$\begin{bmatrix} R' \\ G' \\ B' \end{bmatrix} = \begin{bmatrix} 3.240479 & -1.537150 & -0.498535 \\ -0.969256 & 1.875992 & 0.041556 \\ 0.055648 & -0.204043 & 1.057311 \end{bmatrix} \begin{bmatrix} X'' \times 0.950456 \times 255 \\ Y' \times 255 \\ Z'' \times 1.088754 \times 255 \end{bmatrix} \tag{5}$$

3.2 Example and Analysis of Color Correction

Strictly speaking, there are no ideal input images with absolutely no color excursion in the actual collection. The reason is that some factors, such as exposure quality and environment lighting angle, will certainly cause background and face foreground color excursion in various degrees or in different parts. Hence, color excursion correction is a necessary pretreatment

measure before skin modeling and detection is executed. Figure 2 shows two groups of examples and analysis for color excursion correction. Group 1 contains three kinds of input images with obvious red, green, and blue color excursion, while Group 2 contains two kinds of input images (simple background and complex background) with micro color excursion.

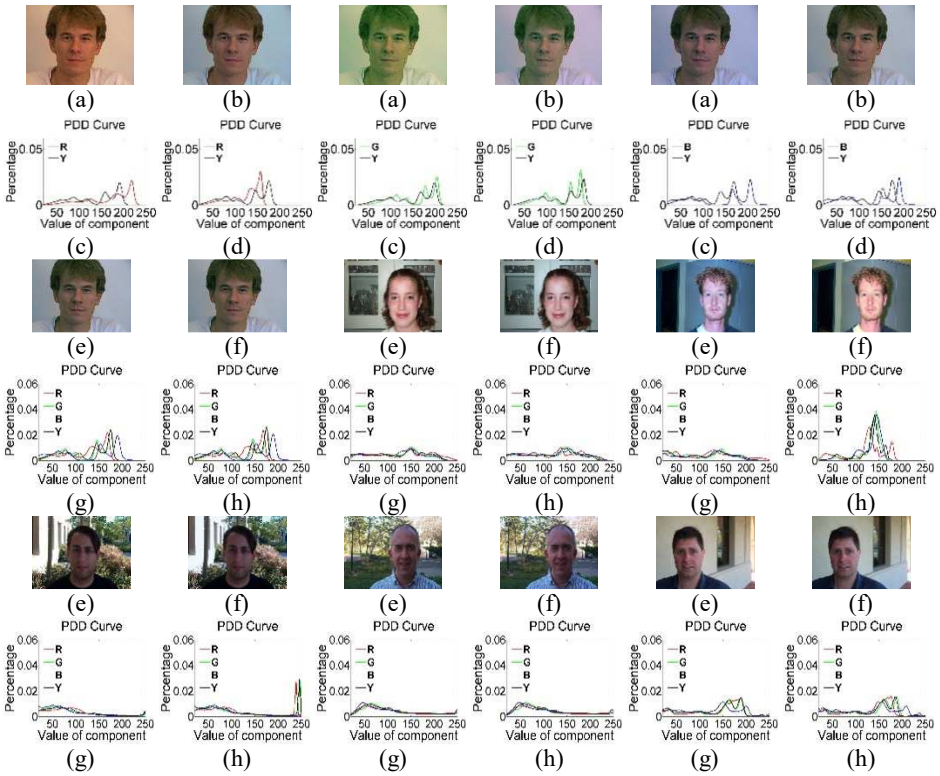

Figure 2 Comparable results and analysis of pretreatment of color excursion correction. (a) Original image with obvious color excursion (red, green, blue); (b) color-corrected image of Figure (a); (c) histogram color-luminance curves of Figure 2(a) (R'/G'/B'-Y"); (d) histogram color-luminance curves of Figure 2(b) (R'/G'/B'-Y"); (e) original image with micro color excursion (simple and complex background); (f) Color-corrected image of Figure (e); (g) histogram color-luminance curves of Figure 2(e) (R'G'B'-Y"); (h) histogram color-luminance curves of Figure 2(f) (R'G'B'-Y") (R'G'B'-Y").

Figure 2(a) represents three input images with obvious color excursion (red, green, blue), Figure 2(b) represent three color-corrected images of Figure 2(a). Figure 2(c) represents three histogram curves of color-luminance components of Figure 2(a) (red curve-R' component, green curve-G' component, blue curve-B' component, black curve-Y' component), Figure 2(d) represents three histogram

curves of the color-luminance components of Figure 2(b). Comparing the images (Figure 2(a) and 2(b)) before and after color excursion correction, as well as comparing their corresponding histogram curves (Figure 2(c) and 2(d)), the heavily shifted colors of the input image with obvious color excursion were reduced well by color excursion correction. The background and skin region in the color-corrected images are easier to distinguish than in the input image.

Figure 2(e) represents two kinds of input images with micro color excursion (simple and complex background), Figure 2(f) represents two kinds of color-corrected images of Figure 2(e). Figure 2(g) represents two kinds of histogram curves of the color-luminance components of Figure 2(e) (red curve-R' component, green curve-G' component, blue curve-B' component, black curve-Y' component). Figure 2(h) represents two kinds of histogram curves of the color-luminance components of Figure 2(f). Comparing the images (Figure 2(e) and 2(f)) before and after color excursion correction, as well as comparing their corresponding histogram curves (Figure 2(g) and 2(h)), the slightly shifted colors of the input image with micro color excursion were depressed well by color excursion correction.

From the above, it is easy to know that for input images with obvious or micro color excursion overly suppressing colors will not cause loss of skin features, or even affect subsequent skin detection and reduce the quality of the image. This is because of the self-adaptation of the pretreatment for the color excursion correction. The main principle is that the color excursion correction makes use of the relative relationship between the three respective averages ($\vec{X}$, $\vec{Y}$, $\vec{Z}$) of the X, Y, Z color components and the average value (cXYZ) of ($\vec{X}$, $\vec{Y}$, $\vec{Z}$). This preserves facial contour details and skin tone features. At the same time, color excursion in different degrees is reduced correspondingly and adaptively in different degrees. From Eqs. (3) and (4) it can be seen that the heavier the color excursion of the input image, the smaller the color adjustment coefficient and the sharper the color adjustment (the greater the color excursion suppression). Vice versa, the slighter the color excursion of the input image, the slighter the color adjustment (the slighter the color excursion suppression).

4 Pretreatment of Luminance-Color Balance

4.1 The Principle and Process of Luminance-color Balance

4.1.1 Lab Color Model

As mentioned in the second section, in addition to the most common RGB model, common color models are HSB, YCbCr, XYZ, CMYK, Lab, and so on

[4-15]. HSB is often used as a temporary model in image processing. YCbCr is often applied in image compression and skin-tone segmentation [5-11]. Lab describes the human visual perception in digital mode. It does not depend on light and pigment and is device-independent. Therefore, it makes up for RGB's deficiency of depending on the color characteristics of the device and its uneven color distribution. This model has a wide color gamut, which not only contains the whole color gamut of RGB and CMYK but also expresses colors they cannot express. That is, the color information that RGB describes can be mapped in Lab space while the color perceived by the naked eye can also be expressed by the Lab color model. The Lab color model is shown in Figure 2, where three components respectively represent L (luminosity, 0~100, from black to white), a (-120~120, from green to red/magenta, negative values -a* indicate green while positive values a* indicate magenta), b (-120~120, from blue to yellow, negative values -b* indicate blue and positive values b* indicate yellow).

Cai, *et al*. introduced the clustering result of skin in CIE Lab color space. They considered that the CIE Lab color space has better cognitive uniformity than RGB and VHS color space [16]. Based on broad characteristics of the color gamut, equalization and richness characteristics of color expression as well as the ability of skin description, this paper proposes a self-adaptive luminance and color-balance function using the a', b' and L' components in Lab color space. As the Lab model is a device-independent color model, the component values obtained by the original conversion method (see Eqs. (6)-(8)) are non-RGB display color data. Making use of a linear normalized mapping method, the L, a, b components can be adjusted to the range of [0,255], which can be displayed by devices (see Eqs. (9)-(10)). The proposed method acquires three adjusted and displayable L', a', b' components based on Eq. (10) and then establishes a self-adaptive nonlinear amendment function in order to balance the luminance and color of the color-corrected image. Conversion of the Lab color components is done as follows:

$$\begin{bmatrix} X \\ Y \\ Z \end{bmatrix} = \begin{bmatrix} 0.412453 & 0.357580 & 0.180423 \\ 0.212671 & 0.715160 & 0.072169 \\ 0.019334 & 0.119193 & 0.950227 \end{bmatrix} \begin{bmatrix} r \\ g \\ b \end{bmatrix} \tag{6}$$

$$\begin{cases} L = 116 \times f(Y_1) - 16 \\ a = 500 \times (f(X_1) - f(Y_1)) \\ b = 200 \times (f(Y_1) - f(Z_1)) \end{cases} \tag{7}$$

$$f(x)=\begin{cases} x^{1/3} & if\,(x>0.008856) \\ (7.787\times x)+(16/116) & else \end{cases} \tag{8}$$

where, r, g, and b are the R', G', B' components corrected by Gamma respectively, X_1, Y_1, and Z_1 are the linearly normalized X, Y, Z components respectively, $f(x)$ is the correction function, and x represents X_1, Y_1, Z_1. The adjustment method of the displayable components is done with Eq. (9). Therein, ca and cb are the adjustment coefficients for the range of a and b. ca = 1.4749, cb = 0.6245. Eq. (9) can be converted to Eq. (10).

$$\begin{cases} L'=Y_1=0.2126\times R'+0.7152\times G'+0.0722\times B' \\ a'=ca\times(X_1-Y_1)+128 \\ b'=cb\times(Y_1-Z_1)+128 \end{cases} \tag{9}$$

$$\begin{bmatrix} L' \\ a' \\ b' \end{bmatrix}=\begin{bmatrix} 0.2126 & 0.7152 & 0.0722 \\ 0.3263953 & -0.4999911 & 0.17359573 \\ 0.12171505 & 0.37825905 & -0.4999747 \end{bmatrix}\begin{bmatrix} R' \\ G' \\ B' \end{bmatrix}+\begin{bmatrix} 0 \\ 128 \\ 128 \end{bmatrix} \tag{10}$$

4.1.2 Self-adaptive Nonlinear Amendment Function

Based on the acquired L', a', b' components calculated by Eq. (10), this study established a self-adaptive nonlinear amendment function in order to balance the luminance and color of the color-corrected image and to improve the skin detection rate in the processing sequence. The traditional Gamma correction method is only appropriate for grayscale images and lacks self-adaptation. It simply adjusts up the low-gray-scale regions and adjusts down the high-gray-scale regions. The adaptive nonlinear amendment function established in this study is an improvement and extension of traditional Gamma correction, which is aimed at the row-column-transformed sub-block image of a color image.

The function limits the influence of the luminance (L') as much as possible. Meanwhile, it makes use of the correlation between the a' and b' components, which are independent of the luminance (L'), and the ability of skin description as well as the relationship between three average values ($\bar{R}'$, $\bar{G}'$, $\bar{B}'$) of R', G', B' and luminance (L'). Moreover, based on the above considerations, a self-adaptive parameter is introduced to calculate and acquire three adaptive correction coefficients. Then, the local self-adaptive nonlinear amendment function is further established with these coefficients in order to amend and balance the local luminance and color of the row-column-transformed sub-block image of the color-corrected image. Thereby, global luminance-color balance of the color-corrected image can be realized. The process of luminance-color balancing is as follows:

1. Make a conversion in the rows and columns of the color-corrected image and acquire the row-column-transformed multi-block image and row-column-transformed sub-block images.
2. Acquire the L', a', b' components of every sub-block image of the color-corrected image according to Eq. (10). With Eq. (11), accumulate the R', G', B' components respectively and compute the averages ($\bar{R}'$, $\bar{G}'$, $\bar{B}'$) of the R', G', B' components in the different sub-images.

$$\bar{R}' = \frac{1}{k^2}\sum_{j=1}^{j=k}\sum_{i=1}^{i=k} R'_{i,j} \ , \ \bar{G}' = \frac{1}{k^2}\sum_{j=1}^{j=k}\sum_{i=1}^{i=k} G'_{i,j} \ , \ \bar{B}' = \frac{1}{k^2}\sum_{j=1}^{j=k}\sum_{i=1}^{i=k} B'_{i,j} \tag{11}$$

where, $k = (w \times h) / 2^n$, i and j are the horizontal and vertical coordinates of a pixel, n is the layer of the row-column transformation (n = 2), k is the number of row-column-transformed sub-block images. Meanwhile, w and h are the length and width of the image.

3. By using the L', a', b' components and the averages ($\bar{R}'$, $\bar{G}'$, $\bar{B}'$) of the R', G', B' components, calculate the self-adaptive amendment coefficients (cR', cG', cB') of every sub-block image with Eq. (12). At the same time, the maximum value (mL') of luminance component (L') in each sub-block image is acquired.

$$\begin{cases} M = \sqrt{0.5 \times [(a'^2 + b'^2)/(a' + b')^2 \ ]} \\ cR' = M^{(L'/\bar{R}')} \ , \ cG' = M^{(L'/\bar{G}')} \ , \ cB' = M^{(L'/\bar{B}')} \end{cases} \tag{12}$$

4. By using the R, G, B components and the self-adaptive blocked amendment coefficients (cR', cG', cB'), as well as luminance L' and the maximum mL' value, establish the local adaptive nonlinear amendment functions (f(R'), f(G'), f(B')) of every sub-block image according to Eq. (13). Use the local adaptive nonlinear amendment functions to amend the R', G', B' components of every sub-block image and realize the local luminance-color balance or amendment.

$$\begin{cases} f(R') = [mL' \times (R' \times cR \ ' / L')^{\ cR'} + cR'] \ , \ R' = \sqrt{R' \times f(R')} \\ f(G') = \ [mL' \times (G' \times cG \ ' / L')^{\ cG'} + cG'], \ G' = \sqrt{G' \times f(G')} \\ f(B') = [mL' \times (B' \times cB \ ' / L')^{\ cB'} + cB'], \ B' = \sqrt{B' \times f(B')} \end{cases} \tag{13}$$

5. Make an inverse conversion in the rows and columns of the sub-block image, which is amended by the local luminance-color balance or amendment, in order to acquire the global color image (luminance-color-balanced image). Then use the parameterized normalization function to stretch the luminance of the global color image (luminance-color-balanced

image) globally to the range of (20, 230) in Lab color space by converting RGB to Lab color format of the global color image, in order to remove highlights (L >= 230) and shadows (L <= 20). Finally, the luminance-stretched luminance-color-balanced image should be obtained for the skin detection sequence.

4.2 Example and Analysis of Luminance-color Balance

In the actual collection there is also no ideal input image with absolute balance of luminance and color. Because of some factors, such as the sags and crests of the human face, the influence of the device and the surrounding environment, imbalance of luminance and color is caused in different degrees or in different parts of the input image. As mentioned before, the principle of pretreatment of the luminance-color balance makes use of the correlation between the L', a', and b' color components as well as the relative relationship between the three averages ($\bar{R}'$, $\bar{G}'$, $\bar{B}'$) and luminance (L') in order to calculate the adaptive local amendment coefficients and establish the adaptive local amendment function for the row-column-transformed sub-block images. Thus, facial contour details and skin tone features are preserved well. At the same time, the different degrees of luminance-color imbalance can be suppressed or balanced.

From Eqs. (11)-(13), it can be seen that the greater the local luminance-color imbalance of the sub-block image, the greater the local amendment function's suppression degree of luminance-color imbalance. Conversely, the smaller the local luminance-color imbalance of the sub-block image, the smaller the suppression degree of luminance-color imbalance of the sub-block image. Thus, for the input image with less obvious luminance-color imbalance (the absolute ideal condition usually does not exist) it will not happen easily that excessive suppression results in loss of skin tone characteristics and negatively influences skin detection.

Figure 3 shows examples and analysis of color excursion correction as well as luminance-color balance for three groups of images with obvious color excursion (red, green, and blue), micro color excursion, and less obvious luminance-color imbalance. The image in Figure 3(b) (or Figure 3(k)) (color-corrected images) was processed successively by two-layer (n = 2) row-column transformation and local luminance-color balance, and then the luminance-color-balanced multi-block image was acquired, as shown in Figure 3(c) (or Figure 3(l)). After row-column inverse transformation of the sub-block image into a multi-block image, and normalizing or stretching the luminance, the luminance-color-balanced image and the luminance-stretched luminance-color-balanced image were acquired, as shown in Figure 3(d) (or Figure 3(m)) and Figure 3(e) (or Figure 3(n)).

Comparing the color-brightness histogram curves of the color-corrected image and the luminance-stretched luminance-color-balanced image (also called the preprocessed image) (see Figure 3(g) and 3(i), or Figure 3(p) and 3(r)), the peak value of the PDD (probability density distribution) curve of the luminance Y" component in Figure 3(i) (or Figure 3(r)) was closer to the medium gray level than that in Figure 3(g) (or Figure 3(p)).

This means that the number of pixels with high brightness or low brightness was decreased. Thus, highlights and shadows were suppressed and the two peaks of the R', G', B' color components can be distinguished more clearly. Comparing the color-corrected images and the luminance-stretched luminance-color-balanced images, it is also easy to see that even though the images (with obvious color excursion, micro color excursion, or less obvious luminance-color imbalance) were processed by luminance-color balancing, the unequal luminance and color of face and background were balanced adaptively in different degrees.

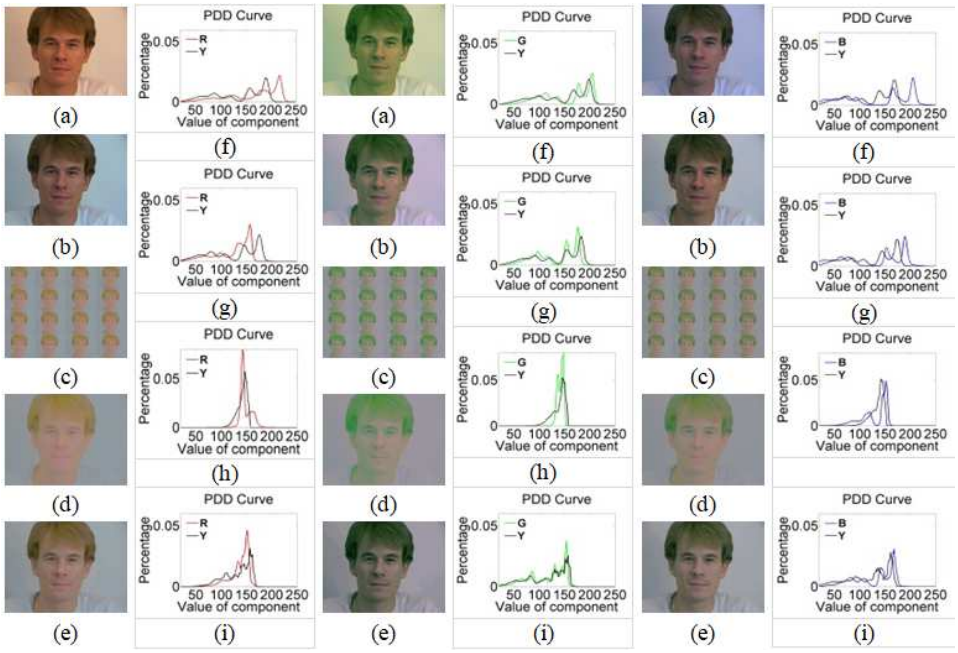

Figure 3 Preprocessing and analysis of color excursion and luminance-color balance.

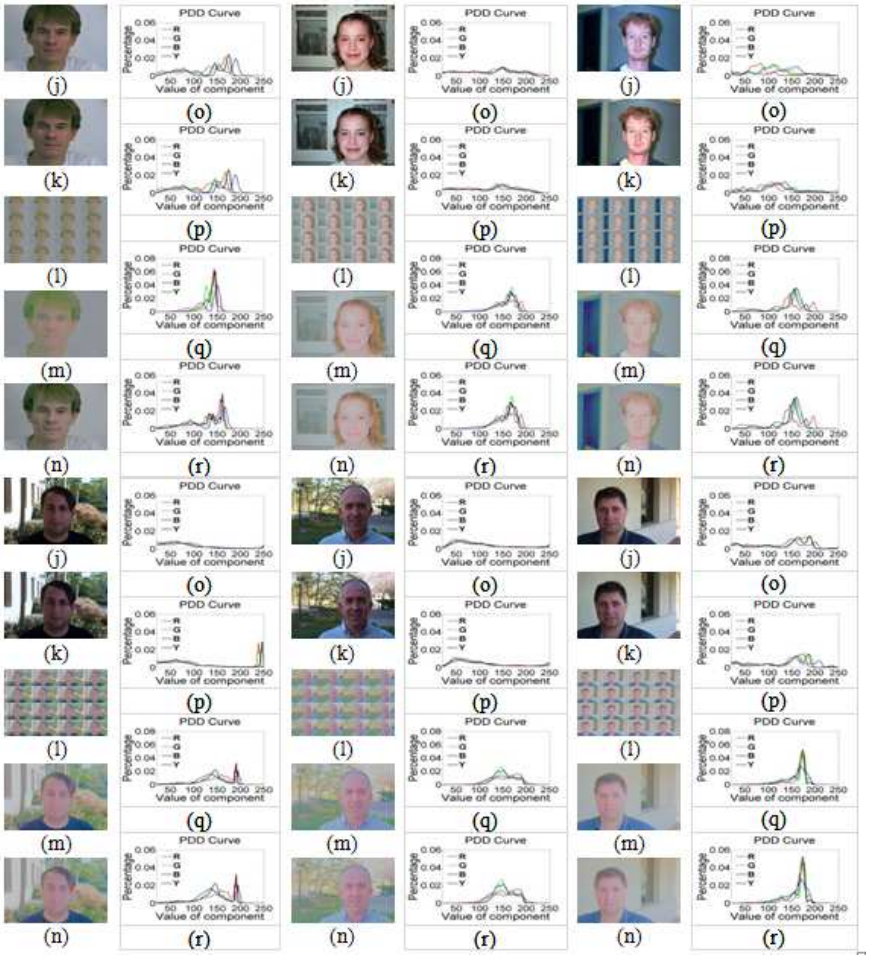

Figure 3 ***Continued.*** Preprocessing and analysis of color excursion and luminance-color balance. (a) Original images with obvious color excursion (R/G/B); (b) color-corrected images of (a); (c) block-processed images of (b); (d) luminance-color-balanced images of (b); (e) luminance-stretched luminance-color-balanced images of (b); (f) color-brightness histogram curves of (a) (R'/G'/B'-Y"); (g) color-brightness histogram curves of Figure (b) (R'/G'/B'-Y"); (h) color-brightness histogram curves of (d) (R'/G'/B'-Y"); (i) color-brightness histogram curves of (e) (R'/G'/B'-Y"); (j) original images with micro color excursion or less obvious luminance-color imbalance; (k) color-corrected images of (j); (l) block-processed images of (k); (m) luminance-color-balanced images of (k); (n) luminance-stretched luminance-color-balanced images of (k); (o) color-brightness histogram curves of (j) (R'G'B'-Y"); (p) color-brightness histogram curves of (k) (R'G'B'-Y"); (q) color-brightness histogram curves of (m) (R' G' B'-Y"), (r) color-brightness histogram curves of (n) (R'G'B'-Y").

The too dark and too bright areas were also balanced and weakened, and the important or key facial features (e.g. skin target boundary, eyes, mouth) were preserved as far as possible, which is beneficial for skin detection. Meanwhile, for the images with micro color excursion and normal skin tone as well as for the images with less obvious luminance-color imbalance, excessive suppression causing loss of skin tone characteristics did not occur.

5 Skin Modeling and Detection

5.1 Principle of Skin Detection based on L'a'b' 3D Semi-supervised Dual-probability Skin Model

As stated in Section 3.1, the Lab color model has a broad color gamut, rich and balanced colors, as well as good ability of skin description. Caj, *et al.* argued that Lab color space has better cognitive uniformity than RGB in accordance with skin clustering results [16]. Ref. [1] compared the distribution situation of highlight face skin tone in two-dimensional planes in multiple color space. From this it can be known that, in various distributions of typical color spaces, luminance-uneven skin images have the smallest overall proportion of skin area in La*b* 3D space and the smallest single ratio of skin area in a*b* 2D color space separated by luminance (L). Ordinarily, the smaller the proportion of skin area, the easier it is to separate skin and non-skin regions.

Based on the MIT-CBCL [23] + Caltech [24] face databases, statistical analysis of cluster distributions in L'a'b' color space was carried out for skin targets (a total of 2861633 skin tone points) and non-skin targets (a total of 11918729 skin tone points), respectively, on preprocessed (color-corrected and luminance-color-balanced) face image samples. Cluster distribution of skin tone has an ellipsoidal shaped concentration distribution in L'a'b' 3D space and has an elliptical concentration distribution in a'b' 2D space separated from luminance (L'), as shown in Figure 4. Thus, by the 3D coordinate parameters of the statistical ellipsoid barycenter, we established an L'a'b' 3D semi-supervised dual-probability skin model in order to calculate skin similarity, formulated by the following Eq. (14):

$$\begin{cases} S_{i,j} = \dfrac{x^2}{31.305^2} + \dfrac{y^2}{20.125^2} + \dfrac{z^2}{200^2}, \\ S'_{i,j} = \dfrac{x'^2}{31.305^2} + \dfrac{y'^2}{20.125^2} + \dfrac{z^2}{200^2}, \\ P_{i,j} = \dfrac{S_{i,j} + S'_{i,j}}{2} \le 1 \end{cases} \tag{14}$$

where , $S_{i,j}$ and $S'_{i,j}$ are skin similarity 1 and similarity 2 of the current pixel.

$$x=\frac{a'-150\times\left[1+\frac{(a'-\bar{a}')}{\bar{a}'}\times\frac{(L'-\bar{L}')}{\bar{L}'}\right]}{\cos(\pi/4)},x'=\frac{a'-148\times\left[1+\frac{(a'-\bar{a}')}{\bar{a}'}\times\frac{(L'-\bar{L}')}{\bar{L}'}\right]}{\cos(\pi/4)}$$

$$y=\frac{b'-130\times\left[1+\frac{(b'-\bar{b}')}{\bar{b}'}\times\frac{(L'-\bar{L}')}{\bar{L}'}\right]}{\cos(\pi/4)},y'=\frac{b'-136\times\left[1+\frac{(b'-\bar{b}')}{\bar{b}'}\times\frac{(L'-\bar{L}')}{\bar{L}'}\right]}{\cos(\pi/4)}$$

$z=(L'-200),z'=(L'-200)$. L', a', and b' are the three components of the current pixel in position (i, j). The $\bar{L}'$, $\bar{a}'$, and $\bar{b}'$ are averages of L', a', and b'. $P_{i,j}$ is the skin similarity of the current pixel. The smaller $P_{i,j}$ is, the larger the probability of skin.

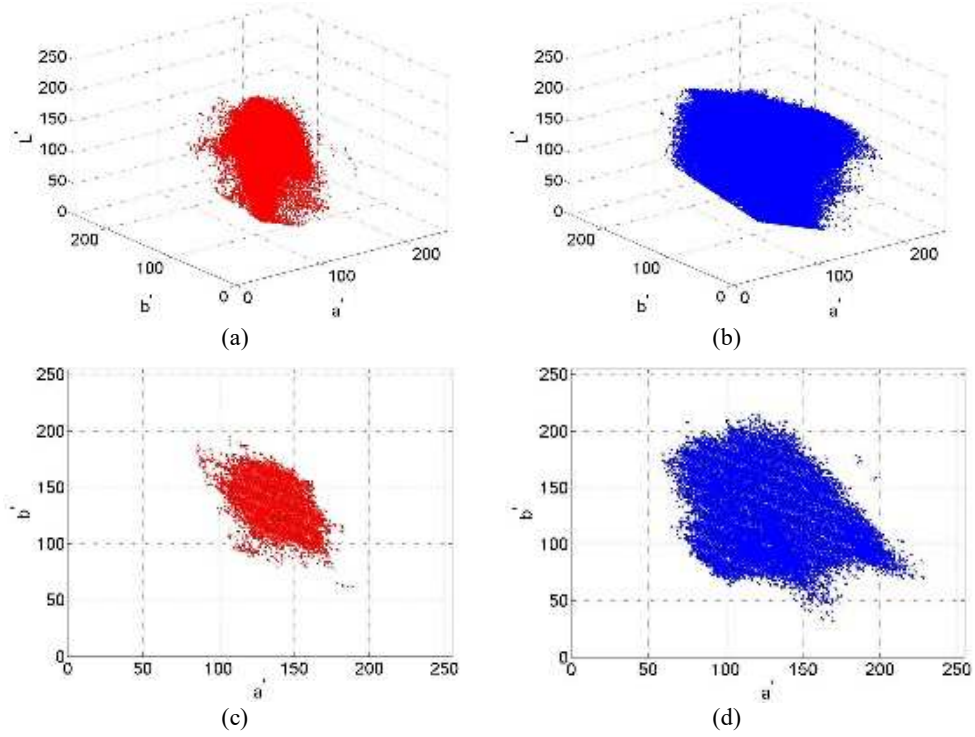

Figure 4 Analysis of cluster skin tone distribution. (a) Cluster distribution of skin tone in L'a'b' space; (b) cluster distribution of non-skin tone in L'a'b' space; (c) cluster distribution of non-skin tone in a'b' space; (d) cluster distribution of non-skin tone in a'b' space.

Based on the established L'a'b' 3D skin model according to Eq. (14), the skin probability can be calculated by Eq. (15). A grayscale similarity image in which the similarity values are compressed to a range of [0 255] can be acquired. With Eq.(16), the skin-detected image can be acquired making use of a dual threshold and binary segmentation. Therein, $P_{i,j}$ is the fused skin probability of the current pixel. $P'_{i,j}$ is the current pixel value in the fused skin similarity image. $P''_{i,j}$ is the current pixel value in the skin-detected binary-segmented image.

$$P'_{i,j} = \begin{cases} 255 & if\,(P_{i,j} \succ 5) \\ P_{i,j} \times 0.2 \times 255; \end{cases} \tag{15}$$

$$P''_{i,j} = \begin{cases} 255 & if\,(P_{i,j} \le 1) \\ 0 & else \end{cases} \tag{16}$$

5.2 Example and Analysis of Skin Detection

Figure 5 shows analysis examples of skin similarity images and skin-detected images corresponding to an R, G, B three-color excursion input image, a micro-color-excursion input image, and an input image with less obvious illumination-color imbalance. The skin detections were based on the three following methods:

Method 1: nonlinear section transformation [6] + CbCr ellipse model [6]
Method 2: proposed pretreatment + CbCr ellipse model [6]
Method 3: proposed pretreatment + L'a'b' 3D model (see Eq.(14))

Figure 5, Figure 5(c) and 5(g) show skin-similarity images and skin-detected images that were acquired by processing the original images with obvious color excursion (Figure 5(a)) using Method 1. Figures 5(d) and 5(g) are skin-similarity images and skin-detected images that were acquired by processing the preprocessed images (color-excursion-corrected and luminance-color-balanced images,

Figure 5(b)) using Method 2. Figures 5(e) and 5(i) are skin-similarity images and skin-detected images that were acquired by processing the preprocess images (Figure 5(b)) using Method 3. Analogously, Figures 5(j)-5(r) are skin-similarity images and skin-detected images that were acquired by processing the original images with micro color excursion (Figure 5(j)) using Methods 1, 2, and 3 respectively.

Figure 5(s)-(θ) are skin-similarity images and skin-detected images that were acquired by processing the original images with less obvious illumination-color

imbalance (Figure 5(s)) using Methods 1, 2, and 3. By comparing Figures 5(c), 5(d) with 5(e) (or comparing Figures 5(l), 5(m), with 5(n), or comparing 5(u), 5(v) with 5(w)), it is plain that the CbCr ellipse model combined with the pretreatment technology proposed in this paper can describe skin tone better than the traditional CbCr ellipse model, while the L'a'b' 3D model combined with the proposed pretreatment technology in this paper can improve the ability of skin-tone description. From the contrast between the three curves, it can be seen that the acquired dual peak features of the histogram curve of the graytone similarity image using Methods 2 and 3 after pretreatment processing were more obvious.

The curve acquired by Method 3 is the smoothest and its dual peak can be distinguished more obviously. This indicates that Method 3 can distinguish skin tone and non-skin tone targets better. Three skin-detected images (Figure 5(g), 5(h) and 5(i), or Figure 5(p), 5(q), and 5(r), or Figure 5(y), 5(z) and 5(θ)) based on the three methods show that the detection effects based on Method 2, which had more true skin tone and less non-skin tone, were better than based on Method 1. Meanwhile, the detection effects based on Method 3 were better than based on Method 2, as Method 3 improved the detection accuracy and reduced over-segmentation and under-segmentation.

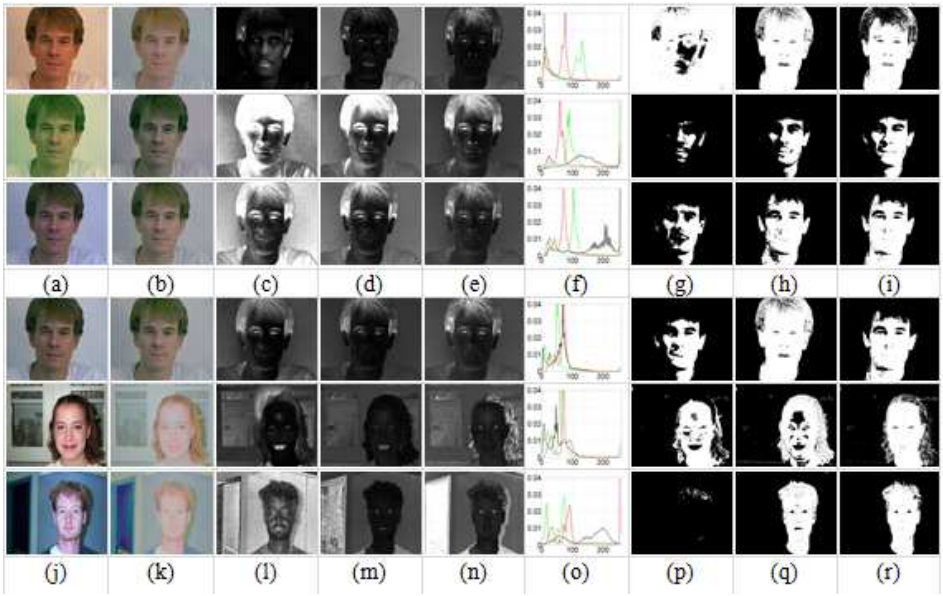

Figure 5 Three kinds of detection results and analysis of three skin models.

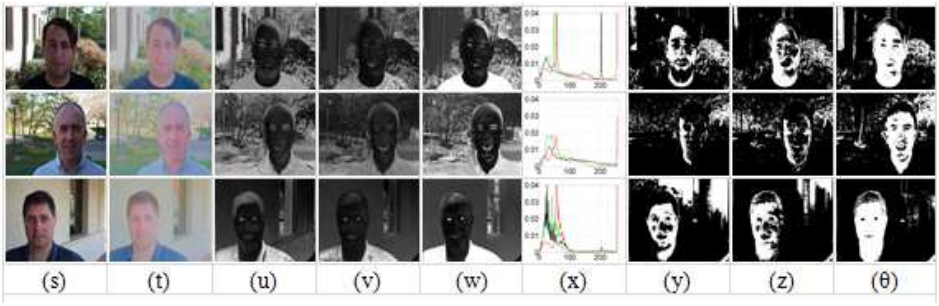

Figure 5 ***Continued.*** Three kinds of detection results and analysis of three skin models. (a) Original images with obvious color excursion (red, green, blue); (b) preprocessed images of Figure 5(a); (c) skin-similarity images of Figure 5(a) based on method 1; (d) skin-similarity images of Figure 5(b) based on method 2; (e) skin-similarity images of Figure 5(b) based on method 3; (f) three kinds of gray histogram curves of three skin-similarity images (black: Figure 5(c), green: Figure 5(d), red: Figure 5(e)); (g) skin-detected images of Figure 5(a) based on method 1; (h) skin-detected images of Figure 5(b) based on method 2; (i) skin-detected images of Figure 5(b) based on method 3; (j) original images with micro color excursion; (k) preprocessed images of Figure 5(j); (l) skin-similarity images of Figure 5(j) based on method 1; (m) skin-similarity images of Figure 5(k) based on method 2; (n) skin-similarity images of Figure 5(k) based on method 3; (o) three kinds of gray histogram curves of three skin-similarity images (black: Figure 5(l), green: Figure 5(m), red: Figure 5(n)); (p) skin-detected images of Figure 5(j) based on method 1; (q) skin-detected images of Figure 5(k) based on method 2; (r) skin-detected images of Figure 5(k) based on method 3; (s) original images with less obvious luminance-color imbalance; (t) preprocessed images of Figure 5(s); (u) skin-similarity images of Figure 5(s) based on method 1; (v) skin-similarity images of Figure 5(t) based on method 2; (w) skin-similarity images of Figure 5(t) based on method 3; (x) three kinds of gray histogram curves of three skin-similarity images (black: Figure 5(u), green: Figure 5(v), red: Figure 5(w)); (y) skin-detected images of Figure 5(s) based on method 1; (z) skin-detected images of Figure 5(t) based on method 2; (θ) skin-detected images of Figure 5(t) based on method 3.

6 Experimental Result

6.1 Experimental Conditions and Analysis

In the skin test experiments, the adopted test face images were acquired from MIT-CBCL Face Database [23], Caltech Face Datasets [24], Georgia Tech Face Database [25], University of Oulu Physics-based Face Database [26], while some images came from autodyne and network. These images include 150 images with normal skin tone (from MIT-CBCL + Caltech), 150 images with unequal luminance and color excursion (from MIT-CBCL + Caltech +

University of Oulu), 150 images with complex interference background (acquired from Caltech + Georgia Tech), as well as 50 images with complex interference, multiple poses and multiple faces (from autodyne and network). The experimental platform was P4 PC + Win 7 + VC 6.0 + Matlab 7.0.

Figure 6 shows examples of skin detection (normal skin tone face, single face with unequal luminance and color excursion, single face or multiple faces with complex background).

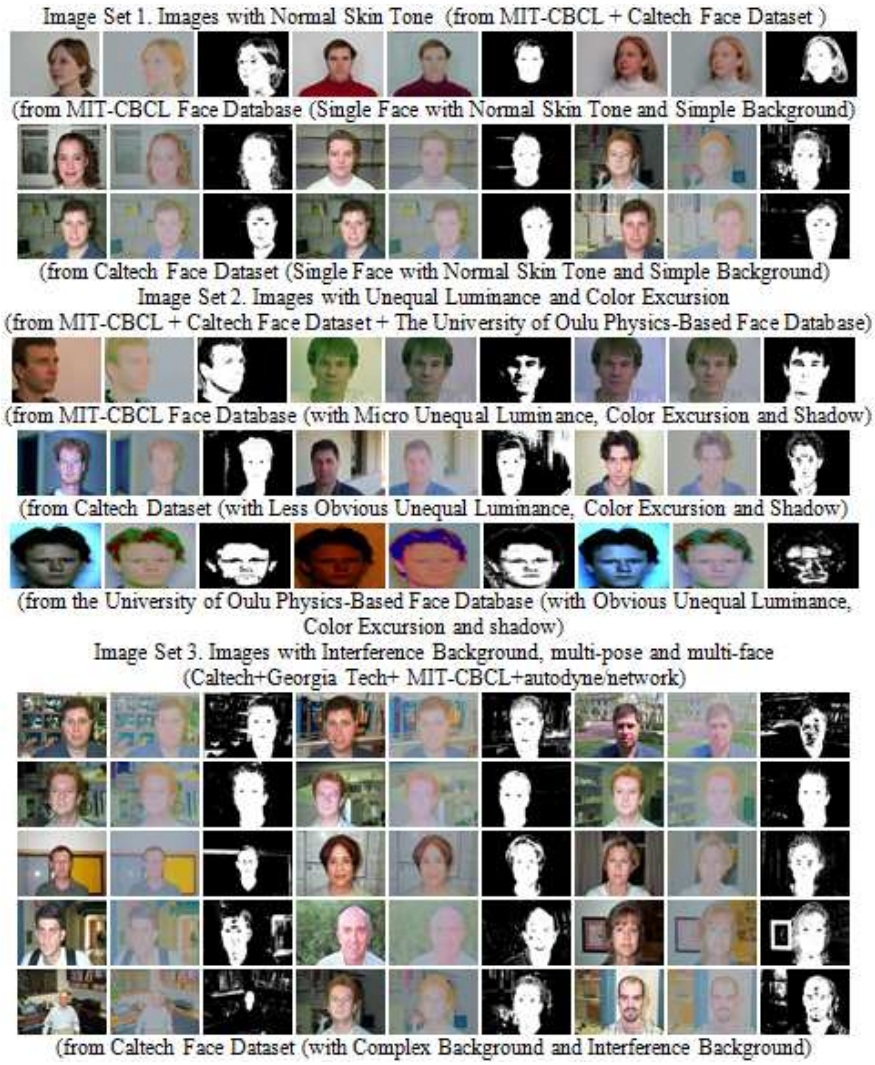

Figure 6 Examples of skin detection.

Figure 6 ***Continued.*** Examples of skin detection. (a) Original images; (b) preprocessed images; (c) skin-detected images using proposed method (3).

Table 1 and 2 respectively showed the detection rate and the average completion time of processing.

Table 1 Comparisons of skin detection rate (CDR % / FDR %).

Detection Method / Type of Image Set	**Normal Skin Tone**	**Unequal Luminance and Color Excursion**	**Interference Background, Multi-pose and Multi-face**
Face database [23-26]	Database 1[1]	Database 2[2]	Database 3[3]
images	150	150	200
Method 1[4]	86.2/15.3	84.3/8.2	80.5/15.6
Method 2[5]	92.9/7.2	91.5/7.8	85.6/14.7
Method 3[6]	93.4/6.7	85.9/8.8	83.8/15.4
Method 4[7]	96.3/5.9	92.5/6.9	89.4/8.7
Method 5[8]	97.4/4.8	93.6/5.7	91.2/7.6

[1] MIT-CBCL + Caltech Face Database.
[2] MIT-CBCL + Caltech + Oulu Physics-Based Face Database.
[3] Caltech + Georgia Tech + autodyne/network.
[4] CbCr Threshold Method [7].
[5] Gaussian Model Method [8-9].
[6] Nonlinear section transformation [6] + CbCr ellipse model [6].
[7] Proposed pretreatment + CbCr ellipse model [6].
[8] Proposed pretreatment + L'a'b' 3D model (see Eq. (14)).

Table 2 Average time per phase of detection (s) (250×250 pixels).

Processing Phase / Type of Image Set	Color Excursion Correction	Luminance-Color Balance	Skin Detection	Total Time Consuming
Normal skin tone (less obvious luminance-color imbalance)	0.009	0.243	0.026	0.278
Unequal luminance and color excursion	0.014	0.358	0.038	0.410
Background interference	0.016	0.402	0.046	0.464

The correct detection rate (CDR) [15] represents the probability of a pixel to be correctly detected, while the false detection rate (FDR) [15] represents the probability of a pixel to be wrongly detected, as shown in Eqs. (17) and (18). TP is true positive (ground truth skin & classified skin), TN is false negative (ground truth skin & classified non-skin), FP is false positive (ground truth non-skin & classified skin), TN is true negative (ground truth non-skin & classified non-skin) [12].

$$CDR = \frac{TP + TN}{TP + TN + FP + FN} \tag{17}$$

$$FDR = \frac{FP + FN}{TP + TN + FP + FN} \tag{18}$$

From Tables 1 and 2, performances (CDR / FDR and time consumption) of the method with CbCr threshold, the method with Gaussian model, the method with CbCr ellipse model, and the method proposed in this paper performed differently on different image types. This is because each skin model has different degrees of sensitivity to different image sets. By comparison, unequal luminance and color excursion may reduce the correct rate of skin detection, while targets with an approximate skin tone (or non-skin tone) may reduce the detection rate and increase the error detection rate. Using the pretreatment measure, unfavorable factors such as color excursion or luminance-color imbalance can be decreased further. Thus, the proposed pretreatment method is beneficial for improving the skin detection rate. Meanwhile, modeling using the skin model proposed in this paper and segmenting skin targets based on this model can improve the detection rate and decrease the detection error rate.

This method can scale a face image with 5 million pixels into 250×250 pixels to process it. The average total time consumption is 0.278~0.464 s. The average memory usage is 8M~11M. The experiment showed that the proposed method had a higher skin detection rate and speed for unequal luminance and color excursion face images than the two other methods.

7 Conclusion

Skin detection of face images with unequal luminance, color excursion and background interference is challenging. This article presented an effective self-adapting method of skin detection that increases the detection rate and interference immunity. This method includes a new pretreatment method and a new L'a'b' 3D skin model was established to calculate the degree of pixel skin similarity for achieving rapid and effective skin detection. The experiment demonstrated that the proposed skin detection method had a high detection rate, good anti-interference ability and adaptability, as well as good real-time performance and practicability.

Acknowledgments

This work was supported by the Scientific Research Foundation of the Education Department of Sichuan Province of China (No. 17ZB0430), the Cooperative Production and Learning and Collaborative Education Project of the Ministry of Education (No. 201702018062), the Meritocracy Research Fund of China West Normal University (No. 17YC154), the Educational Reform Project of China West Normal University (No. JGXMYB18178), and Key Program of General Education Research Fund of Sichuan Province of China (Research on Teaching Reform of IOT Professional Courses in Big Data and AI Era, Sichuan Education letter (2018) No. 495).

References

[1] Voulodimos, A., Doulamis, N., Doulamis, A. & Protopapadakis, E., *Deep Learning for Computer Vision: A Brief Review*, Computational Intelligence and Neuroscience, **2018**, Article No. 7068349, 13 pp., 2018.

[2] Luu, K., Zhu, C., Bhagavatula, C., Le, T.H.N. & Savvides, M., *A Deep Learning Approach to Joint Face Detection and Segmentation [M]*, Advances in Face Detection and Facial Image Analysis, Springer International Publishing, 2016.

[3] Zuo, H., Fan, H., Blasch, E. & Ling, H., *Combining Convolutional and Recurrent Neural Networks for Human Skin Detection*, IEEE Signal Processing Letters, **24**(3), pp. 289-293, 2017.

[4] Chen, D-S. & Liu, Z-K., *A Method for Automatic Detection and Correction of Highlighted Area in Color Face Image*, Journal of Software, **14**(11), pp. 1900-1906, 2003.

[5] Chen, D.G-Y. & Wang, X.G., *Adaptive Illumination Compensation Algorithm for Face Detection,* Computer Engineering and Applications, **48**(22), pp.175-178, 2012.

[6] Hsu, R.L., Abdel-Mottaleb, M. & Jain, A.K., *Face Detection in Color Images*, IEEE Transactions on Pattern Analysis and Machine Intelligence, **24**(5), pp. 696-706, 2002.

[7] Xue, W., Liang, J-D. & Lin, J-X., *AAM Facial Feature Localization Algorithm Based on Skin Model and Breadth-First Search*, Computer Science, **38**(8), pp. 275-276, 2011.

[8] Yuan, W-Q. & Han, C-X., *Multi-Face Detection Algorithm in Complex Background*, Journal of Computer Applications, **30**(3), pp. 635-636, 2010.

[9] Shih, F.Y., Cheng, S.X. & Chuang, C.F., *Extracting Faces and Facial Features from Color Images*, International Journal of Pattern Recognition and Artificial Intelligence, **22**(3), pp. 515-534, 2008.

[10] Wang, Z. & Li, S., Face *Recognition Using Skin Color Segmentation and Template Matching Algorithms*, Information Technology Journal, **10**(12), pp. 2308-2314, 2011.

[11] Liu, Q. & Peng, G.Z., *A Robust Skin Color Based Face Detection Algorithm*, In Proc. 2010 2nd Inter. Asia Conf. Informatics in Control, Automation and Robotics, March 6-7, Wuhan, China, 2010.

[12] Jairath, S., Bharadwaj, S., Vatsa, M. & Singh, R., *Adaptive Skin Color Model to Improve Video Face Detection*, Machine Intelligence and Signal Processing, Springer, New Delhi, pp.131-142, 2016.

[13] Mahmoodi, Reza, M., Sayedi, S.M. & Karimi, F., *Color-Based Skin Segmentation in Videos Using A Multi-Step Spatial Method*, Multimedia Tools and Applications, **76**(7), pp. 9785-9801, 2017.

[14] Mahmoodi, M.R. & Sayedi, S.M., *A Comprehensive Survey on Human Skin Detection*, International Journal of Image, Graphics and Signal Processing, **8**(5), pp. 1-35, 2016.

[15] Kakumanu, P., Makrogiannis, S. & Bourbakis, N., *A Survey of Skin-color Modeling and Detection Methods*, Pattern Recognition, **40**(3), pp. 1106-1122, 2007.

[16] Cai, J. & Goshtasby, A., *Detecting Human Faces in Color Images*, Image and Vision Computing, **18**(1), pp. 63–75, 1999.

[17] Xie, Q.R. & Geng, G.H., *Automatic Face Detection in Video Sequences in Complex Lighting Environments*, Computer Science. **38**(10), pp. 267-269, 2011.

[18] Wang, B., Li, W.F. & Yang, W.M., *Illumination Normalization Based on Weber's Law With Application to Face Recognition*, IEEE Signal Processing Letter, **18**(8), pp. 462-465, 2011.

[19] Cheng, Y., Jiao, L., Cao, X. & Li, Z., *Illumination-Insensitive Features for Face Recognition*. Vis. Comput. **33**(11), pp. 1483–1493, 2017.

[20] Mahmoodi, M.R. & Sayedi, S.M., *A Face Detection Method Based on Kernel Probability Map*. Computers & Electrical Engineering, **46**, pp. 205-216, 2015

[21] Chu, Y., Zhao, L. & Ahmad, T., *Multiple Feature Subspaces Analysis for Single Sample Per Person Face Recognition,* The Visual Computer, **34(**1), pp. 1-18, 2018.

[22] Yong, L. & Guan, Y.P., *Adaptive Skin Detection Using Face Location and Facial Structure Estimation,* IET Computer Vision, **11**(7), pp. 550-559, 2017.

[23] *MIT-CBCL Face Recognition Database*, available: http://cbcl.mit.edu/software-datasets/heisele/facerecognition-database.html. (March 11th, 2018)

[24] *Caltech Face Dataset,* available : http://www.vision.caltech.edu/Image_Datasets/faces/faces.tar. (May 25th, 2018)

[25] *Georgia Tech Face Database*, available: http://www.anefian.com/research/gt_db.zip. (May, 25th, 2018)

[26] *The University of Oulu Physics-Based Face Database*, available: http://www.cse.oulu.fi/CMV/Downloads/Pbfd#Image_Acquisition (May 25th, 2018)